Optical Materials 156 (2024) 115912

Contents lists available at ScienceDirect

Optical Materials

journal homepage: www.elsevier.com/locate/optmat

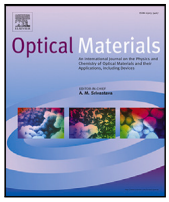

Research article

Enhanced photoluminescence of organic dyes embedded in sol-gel organosilane thin films

Francesco Floris [a,*], Cristiana Figus [b], Francesco Quochi [b], Franco Marabelli [a]

[a] Dipartimento di Fisica, Università di Pavia, Via Agostino Bassi, 6, Pavia, 27100, Italy
[b] Dipartimento di Fisica, Università d Cagliari, S.P. Monserrato-Sestu Km 0,700, Monserrato, 09042, Cagliari, Italy

ARTICLE INFO

Keywords:
Sol–gel
Photoluminescence
Decay time
Organic dye

ABSTRACT

We investigated photoluminescence properties of Dyomics dyes DY650 and DY831 when incorporated into solid thin films fabricated using two distinct sol–gel precursors, namely, tetraethoxysilane (TEOS) and 3-glycidoxypropyltrimethoxysilane (GPTMS). Surprisingly, a significant enhancement in both photoluminescence lifetime and quantum yield was observed in the films derived from GPTMS, contrasting conventional behavior documented in literature for dyes dispersed within solid matrices. This phenomenon is attributed to the unique molecular environment surrounding the dyes in the GPTMS matrix, which was inferred to suppress nonradiative decay channels for the photoexcited dyes. Our findings provide valuable insights into the intricate interplay between dye molecules and their host matrices, shedding light on the potential applications of GPTMS-based systems in enhancing photoluminescence properties for various technological advancements.

1. Introduction

The sol–gel process finds extensive applications in coating preparation across various domains [1].

Notably, coatings derived from tetraethoxysilane (TEOS) and 3-glycidoxypropyltrimethoxysilane (GPTMS) have garnered attention for catalysis, anti-corrosion measures [2,3], self-healing capabilities [4], tissue engineering scaffolds [5], sensors [6–8], unconventional environments [9], and protective coatings [10]. Their stability against photoluminescence (PL) processes makes them suitable as matrix materials for dye embedding, owing to their control over refractive index [11–13], a parameter significantly influencing PL behavior, particularly radiative lifetime [14–16]. Various interconnected matrix parameters, such as viscosity and temperature, affecting PL, necessitate thorough investigation [17,18].

Given our interest in elucidating dye-PL interactions with plasmonic modes supported by 2D metasurfaces [19], our aim is to discern the factors influencing dye emission. Understanding and minimizing interactions between the dye and the molecules binding it to the active plasmonic surface are crucial. A nanometric sol–gel layer emerges as a promising solution for embedding the selected dye. This study focuses on identifying a suitable commercial sol–gel precursor for time-resolved PL emission of organic dyes. We assessed the influence of the environment in terms of excited-state (PL) lifetime for two distinct emitting molecules dispersed within two different silica matrices.

During this analysis, we observed unexpected behavior in GPTMS films concerning the typical matrix effect observed in solid samples, particularly in comparison to TEOS ones. The selected dyes consist of DY650 and DY831 from Dyomics. These dyes were chosen for their absorption and emission features overlapping with the region of interest defined by the plasmonic mode spectral position supported by the aforementioned 2D metasurface. DY650 exhibits absorption and emission features in the visible part of this region, while DY831 displays absorption and emission more centered in its NIR part. Rhodamine-6G (R6G, Sigma-Aldrich) was used as a reference dye for comparative studies, owing to its well-established fluorescence properties.

2. Experimental details

For solution measurements, dyes were dissolved in ethanol (EtOH) and distilled water (H_2O) at a low concentration of 1.5×10^{-6} mol dm^{-3}. This low concentration was deliberately chosen to mitigate concentration quenching effects on photoluminescence (PL) efficiency and lifetime. The two solvents were chosen being widely used, non-toxic and environmental friendly (ensuring an easy implementation in practical applications). Molecular structures of Dyomics dyes are illustrated in Fig. 1, alongside those of the two sol–gel precursors. The sols were synthesized by blending tetraethoxysilane (TEOS, purity > 99%) or 3-glycidoxypropyltrimethoxysilane (GPTMS, purity ≥ 98%),

* Corresponding author.
E-mail address: francesco.floris@unipv.it (F. Floris).

https://doi.org/10.1016/j.optmat.2024.115912
Received 10 May 2024; Received in revised form 30 July 2024; Accepted 31 July 2024
Available online 8 August 2024

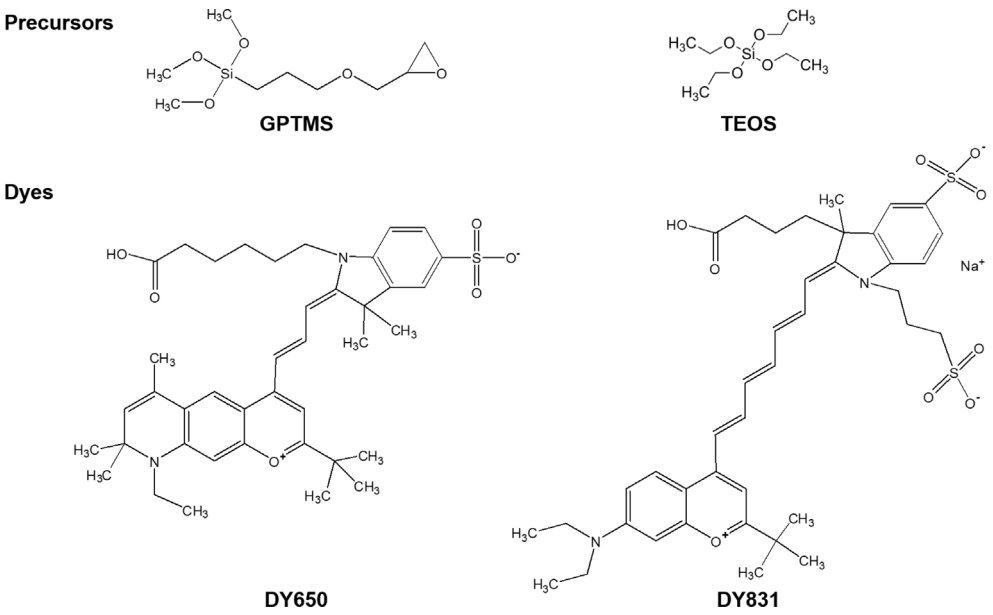

Fig. 1. Sol–gel precursors and dyes. Upper line, GPTMS (left) and TEOS (right). Lower line, DY650 (left) and DY831 (right).

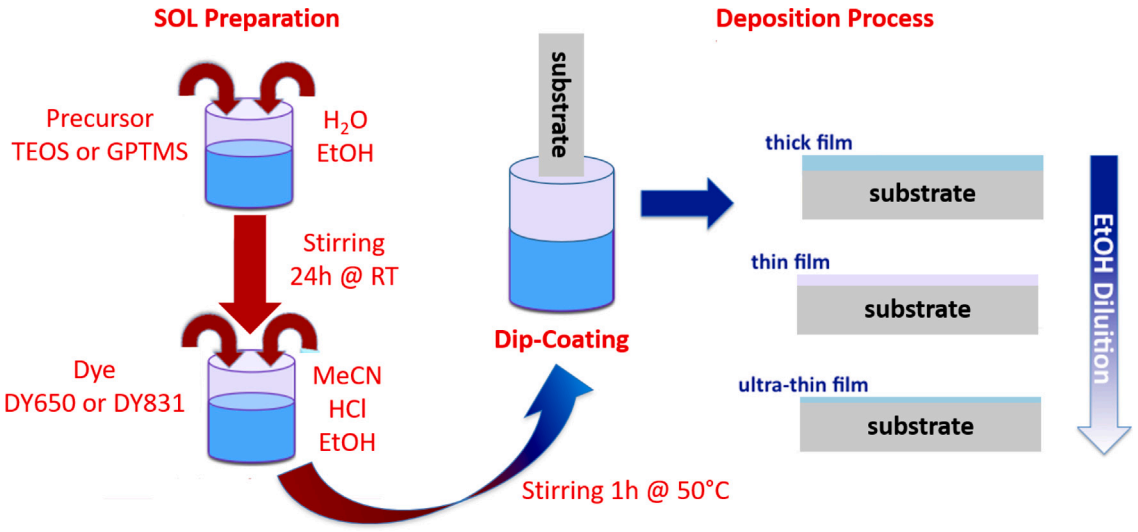

Fig. 2. Scheme of the sol–gel layer fabrication process.

absolute ethanol (EtOH), and distilled water (H_2O) under stirring, with a molar ratio of 1:9.8:5.6, at room temperature (RT) for 24 h. Subsequently, 3 mL of acetonitrile (MeCN) and 3 mL of EtOH were added to 9 mL of the sol. Hydrochloric acid (HCl) was introduced until the pH reached approximately 4, and the mixture was stirred at 50 °C for 1 h. The resulting sol was transferred to a glass vial and cooled to RT. The whole fabrication process is summarized in Fig. 2. Various diluted solutions were prepared by adding further EtOH to the sol. As substrates, soda-lime glasses were chosen and thoroughly cleaned using water, soap, acetone, and finally rinsed with isopropyl alcohol. Dyes were incorporated into the sols at different concentrations, and their content was evaluated in terms of dye/sol–gel precursor molar ratio.

Following the method employed in [20], substrates were immersed in the sol for 25 s. The resulting films were deposited through dip-coating using an ND-R rotary coater (Nadetech Innovations) at a fixed withdrawal speed of 500 mm min-1. The EtOH dilution was varied in the range of 1:15–1:25 (vol vol^{-1}). After deposition, the films were dried at 70 °C for 10 h and then left at RT for 48 h. Film thicknesses were checked by atomic force microscopy (AFM) and ranged from 30 to 50 nm.

Additionally, for control purposes, a further set of films were deposited by drop cast using the lower dye concentrations.

Subsequently, the three resultant doped sol–gel layers were optically excited by frequency-doubled 150-fs pulses (at 392 nm wavelength) from a Ti:Sapphire regenerative amplifier (Quantronix Integra C) operating at a 1 kHz repetition rate. PL signals were spectrally resolved using an Acton SpectraPro 3200i grating spectrometer and time-resolved by a Hamamatsu C5680 streak camera. The PL signal was consistently obtained around the spectrum peak, with a bandwidth of approximately 20 nm in all instances. PL quantum yields (PLQYs) were measured using a Hamamatsu C11347-11 Quantaurus QY instrument. Dye absorbance in thin films was evaluated by Transmittance measurements performed with a UV–VIS-NIR photospectrometer Cary6i Varian.

3. Results and discussion

An investigation of PL lifetime was performed for two Dyomics dyes incorporated in TEOS and GPTMS matrices. A range of dye-to-organosilane molar ratio was explored between 10^{-2} and 10^{-6} mol mol^{-1}. Corresponding PL decay traces are illustrated in Fig. 3.

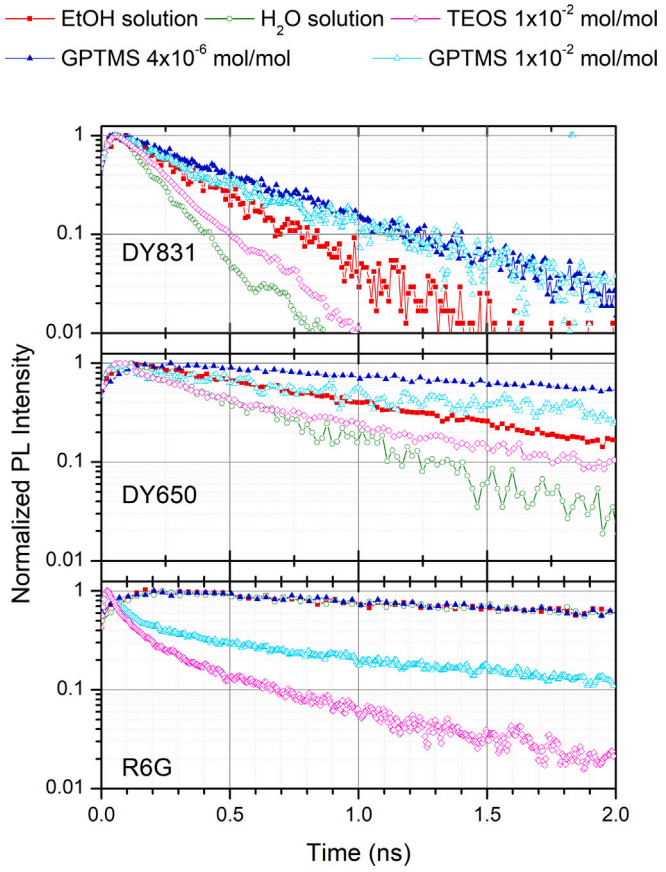

Fig. 3. PL intensity decay traces of Dyomics dyes DY650 and DY831, along with Rhodamine 6G (R6G), in highly diluted EtOH and H_2O solution (1.5×10^{-6} mol dm^{-3}) are represented by red and, respectively, green lines and symbols. The decay traces in TEOS at a dye-to-organosilane molar ratio of 10^{-2} mol mol^{-1} are depicted by magenta lines and symbols, while those in GPTMS at the same molar ratio and at a 4×10^{-6} mol mol^{-1} molar ratio are shown by cyan and blue lines and symbols, respectively. Single exponential decay constants and PLQYs are collected in Table 1.

Reference lifetimes were established for the dyes in highly diluted EtOH solutions to mitigate concentration effects arising from the formation of dimers and higher aggregates. To have a comparison with a second, more polar solvent, results obtained in H_2O solutions have been measured too. In EtOH, both Dyomics dyes displayed a monoexponential PL decay with decay constants of approximately 1.03 ns and 0.30 ns for DY650 and DY831, respectively. With respect to these values, an increase in lifetime was observed in GPTMS for all the explored Dye concentrations.

Concentration levels achieved in the solid state were validated by assessing the PL lifetime of R6G dissolved in both EtOH and organosilane matrices at identical concentrations used for Dyomics dyes. For R6G a significant acceleration of the PL intensity decay, exhibiting a nonexponential profile possibly fitted with a biexponential decay, in the solid matrices at dye-to-organosilane molar ratio of 10^{-2} mol mol^{-1} clearly indicated concentration quenching of the PL emission, possibly due to aggregation effects. The same quenching effect is noticeable for any Dye in TEOS films. Instead, for low concentrations, the PL intensity of R6G exhibits a monoexponential decay in all cases, indicating the attainment of the low concentration limit within the GPTMS matrix. Anyway, PL lifetimes approach, but not exceed the values observed for EtOH solution. On the contrary, for Dyomics dyes, the PL lifetime was confirmed to be longer in the GPTMS matrix compared to solution.

Given these observations, we chose to conduct a thorough evaluation of the PL properties of Dyomics dyes within GPTMS. An evaluation of PLQYs has been possible for DY650 on thick films at exceptionally low concentration levels. This strategy aimed to unequivocally eliminate any potential dye–dye intermolecular interactions, enabling us to isolate and analyze matrix-related effects with precision.

Table 1
Monoexponential PL decay times and PLQYs (in brackets) of dyomics dyes in different solvents and GPTMS matrix at different dye volume concentrations and dye-to-GPTMS molar ratios.

Solvent/matrix (dye concentration/molar ratio)	DY650	DY831
EtOH (1.5×10^{-6} mol dm^{-3})	1.03 ns (21%)	0.30 ns (2.5%)
H_2O (1.5×10^{-6} mol dm^{-3})	0.50 ns (12%)	0.16 ns (–)
GPTMS (4×10^{-6} mol mol^{-1})	2.90 ns (60%)	0.50 ns (–)
GPTMS (8×10^{-5} mol mol^{-1})	2.80 ns (56%)	0.49 ns (–)

PLQYs were found to be roughly proportional to the PL lifetime (see Table 1), demonstrating that enhancement in PL lifetime merely reflects an enhancement in PLQY. This suggests that GPTMS is less effective than liquid solvents in nonradiatively quenching the Dyomics dye PL emission, as clearly occurs in H_2O.

The PL emission spectra of the dye incorporated in GPTMS at two distinct molar ratios are depicted in Fig. 4. At a low molar ratio of 4×10^{-6} mol mol^{-1}, the emission spectrum of DY831 closely resembles that observed in EtOH, contrasting with the blueshifted spectrum for the dye dissolved in H_2O. Conversely, at much higher loading levels (10^{-2} mol mol^{-1}), the spectrum undergoes a noticeable blueshift, indicative of intermolecular interactions between dye molecules rather than self-absorption. This suggests the influence of dye concentration, with $\pi - \pi$ intermolecular interactions commonly recognized as the underlying mechanism behind the pronounced hypsochromic shifts observed in both dye absorption and emission spectra [21,22]. Spectral broadening coexists with blueshift as a potential outcome of configurational disorder inherent in aggregation processes. Similar outcomes were also noted in DY650, albeit to a lesser degree, probably due to its shorter and less elongated molecular structure. To better understand the effect of the molecular structure the Dye optical absorbance was investigated. Fig. 5 reports the Optical Transmittance measured in thin films in GPTMS at the concentration of 10^{-2} mol mol^{-1}. The observed signal is particularly low, but compatible, at least for DY650, with the molar absorbance value of the Dye, its concentration and the small thickness value of the film. In the case of DY831 the signal is even smaller, almost one order of magnitude, meaning a lower Dye and film density. This is consistent, on one side with the small PL signal measured for DY831 samples, on the other side is also consistent with a different molecular arrangement of the (elongated) DY831 in the GPTMS matrix with respect to DY650. Moreover, while the spectral position of the DY650 is in line with the literature data, the absorbance peak in DY831 film appears to be slightly red shifted and becomes largely superimposed with the PL spectra at the same concentration. Furthermore, the blue shift observed in PL spectra indicates a low self absorption effect, probably prevented by the low density of Dye molecules in the film.

Dye aggregation effects were comprehensively monitored through the PL lifetime as a function of the dye-to-GPTMS molar ratio. The data, summarized in Fig. 5, reveal that at molar ratios below 10^{-3} mol mol^{-1}, both Dyomics dyes exist in a low-concentration regime primarily influenced by matrix-related effects. However, at larger molar ratios, the PL lifetime progressively decreases as dye–dye intermolecular interactions emerge due to dye aggregation, causing nonradiative relaxation and hence PL quenching. Notably, an increase in the molar ratio leads to a departure from monoexponential decay of the PL intensity versus time, requiring the reporting of a generalized PL lifetime calculated as the amplitude-averaged decay time of biexponential fit curves. This phenomenon is characteristic of concentration quenching (see Fig. 6).

Based on our experimental results, the elongated structure of the Dyomics dyes, coupled with the superstructure of GPTMS matrix, appears to hinder a close contact and interaction with the host matrix.

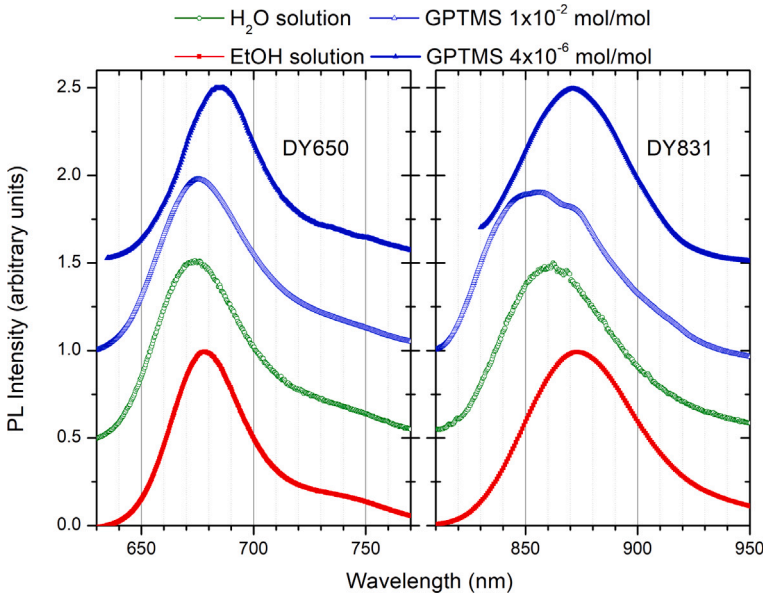

Fig. 4. PL spectra of Dyomics dyes in EtOH and H_2O solutions, and GPTMS matrix with two distinct dye-to- GPTMS molar ratios. The dye volume concentration in solution is 1.5×10^{-6} mol dm^{-3}.

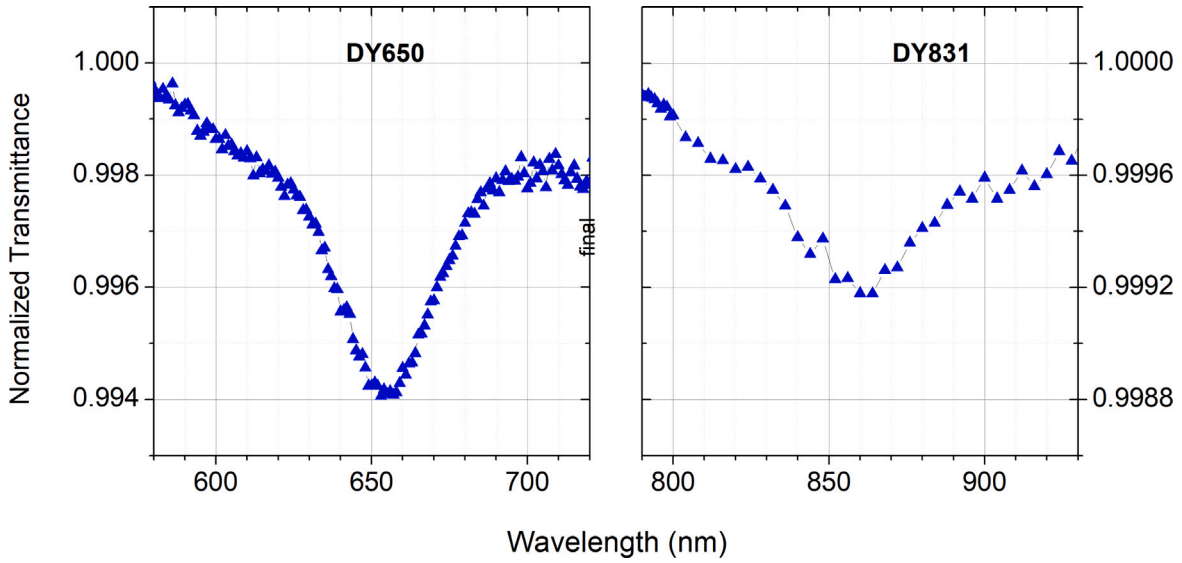

Fig. 5. Optical transmittance spectra of Dyomics dyes DY650 (left panel) and DY831 (right panel).

Consequently, this reduces the introduction of nonradiative deactivation channels for the photoexcited Dyomics dyes, even compared to the EtOH solution. GPTMS appears to alleviate steric hindrance effects, accommodating DY650 and DY831 dyes in a manner that minimizes their interaction with the matrix. However, this effect vanishes as the molar ratio increases, with concentration effects progressively outweighing matrix-related ones.

Interestingly, an observed enhancement in PL intensity was attributed to the hydrophobic nature of GPTMS, which facilitates the creation of a non-polar environment favorable to increasing curcumin solubility and thereby enhancing its PL emission [23]. A similar behavior for GPTMS in the solid state was reported, indicating the absence of the expected PL quenching.

4. Conclusions

In summary, our investigation unveils a remarkable increase in the photoluminescence decay time of Dyomics DY650 and DY831 dyes upon their incorporation into solid thin films fabricated using a sol–gel host matrix with 3-glycidoxypropyltrimethoxysilane (GPTMS) as the precursor. This observed effect diverges from both the expected outcomes outlined in existing literature and the conventional behavior associated with dye emission in solid-state films. The revealed phenomenon provides a significant platform for unraveling and analyzing the intricate interplay among sol–gel precursors, photoluminescence characteristics, and other influential factors, including plasmonic effects.

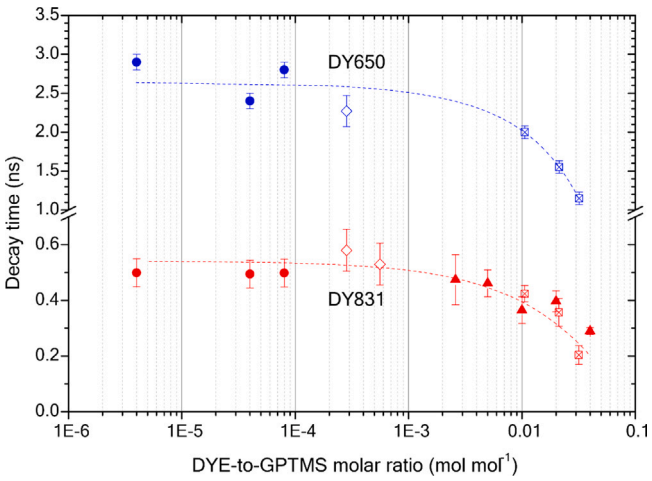

Fig. 6. PL decay times of Dyomics dyes as a function of dye-to-GPTMS molar ratio. DY650 is represented by blue symbols, while DY831 is represented by red symbols. Error bars depict the ensemble standard deviation of measurements conducted at various points within the samples. Different symbols denote distinct sample batches prepared under formally identical conditions.

CRediT authorship contribution statement

Francesco Floris: Writing – review & editing, Writing – original draft, Visualization, Methodology, Investigation, Formal analysis, Conceptualization. **Cristiana Figus:** Investigation, Data curation. **Francesco Quochi:** Writing – review & editing, Writing – original draft, Methodology, Investigation, Formal analysis. **Franco Marabelli:** Writing – review & editing, Validation, Supervision, Methodology, Conceptualization.

Declaration of competing interest

The authors declare that they have no known competing financial interests or personal relationships that could have appeared to influence the work reported in this paper.

Data availability

Data will be made available on request.

References

[1] S. Sfameni, G. Rando, M.R. Plutino, Perspective chapter: Functional sol-gel based coatings for innovative and sustainable applications, in: D.J.P. Singh, D.S.S. Acharya, D.S. Kumar, D.S.K. Dixit (Eds.), Sol-Gel Method - Recent Advances, IntechOpen, Rijeka, 2023, http://dx.doi.org/10.5772/intechopen.110514, (Chapter 3).

[2] J. Li, H. Bai, Z. Feng, Advances in the modification of silane-based sol-gel coating to improve the corrosion resistance of magnesium alloys, Molecules 28 (6) (2023) http://dx.doi.org/10.3390/molecules28062563, URL: https://www.mdpi.com/1420-3049/28/6/2563.

[3] L. Telmenbayar, A.G. Ramu, T.-O. Erdenebat, D. Choi, Anticorrosive lanthanum embedded PEO/GPTMS coating on magnesium alloy by plasma electrolytic oxidation with silanization, Mater. Today Commun. 33 (2022) 104662, http://dx.doi.org/10.1016/j.mtcomm.2022.104662, URL: https://www.sciencedirect.com/science/article/pii/S2352492822015033.

[4] U. Tiringer, A. Durán, Y. Castro, I. Milošev, Self-healing effect of hybrid sol-gel coatings based on GPTMS, TEOS, SiO2 nanoparticles and Ce(NO3)3 applied on aluminum alloy 7075-T6, J. Electrochem. Soc. 165 (5) (2018) C213, http://dx.doi.org/10.1149/2.0211805jes.

[5] M.V. Reyes-Peces, A. Pérez-Moreno, D.M. de-los Santos, M.d.M. Mesa-Díaz, G. Pinaglia-Tobaruela, J.I. Vilches-Pérez, R. Fernández-Montesinos, M. Salido, N. de la Rosa-Fox, M. Piñero, Chitosan-GPTMS-silica hybrid mesoporous aerogels for bone tissue engineering, Polymers 12 (11) (2020) http://dx.doi.org/10.3390/polym12112723, URL: https://www.mdpi.com/2073-4360/12/11/2723.

[6] A. Lobnik, Š.K. Urek, M. Turel, N. Frančič, Sol-gel based optical chemical sensors, in: Optical Sensors 2011; and Photonic Crystal Fibers V, Vol. 8073, SPIE, 2011, pp. 150–160.

[7] T. Zhang, L. Yang, F. Yan, K. Wang, Vertically-ordered mesoporous silica film based electrochemical aptasensor for highly sensitive detection of alpha-fetoprotein in human serum, Biosensors 13 (6) (2023) http://dx.doi.org/10.3390/bios13060628, URL: https://www.mdpi.com/2079-6374/13/6/628.

[8] J. Mrazek, I. Kasik, J. Nekola, T. Martan, O. Podrazky, M. Pospisilova, V. Matejec, Preparation and characterization of sensing layers for pH detection in living plant cells, in: Optical Sensors 2011; and Photonic Crystal Fibers V, Vol. 8073, SPIE, 2011, pp. 254–259.

[9] R.B. Figueira, J.M. de Almeida, B. Ferreira, L. Coelho, C.J.R. Silva, Optical fiber sensors based on sol–gel materials: design, fabrication and application in concrete structures, Mater. Adv. 2 (2021) 7237–7276, http://dx.doi.org/10.1039/D1MA00456E.

[10] L. Cutz, U. Tiringer, W. de Jong, A. Mol, Hybrid sol-gel coatings for reducing wettability and storage degradation of biomass pellets, Mater. Chem. Phys. 304 (2023) http://dx.doi.org/10.1016/j.matchemphys.2023.127861.

[11] G. Wu, J. Wang, J. Shen, T. Yang, Q. Zhang, B. Zhou, Z. Deng, B. Fan, D. Zhou, F. Zhang, A novel route to control refractive index of sol-gel derived nano-porous silica films used as broadband antireflective coatings, Mater. Sci. Eng. B 78 (2–3) (2000) 135–139.

[12] Y. Arai, T. Yano, S. Shibata, High refractive-index thin films derived from organic-inorganic hybrid materials, in: Journal of the Ceramic Society of Japan, Supplement Journal of the Ceramic Society of Japan, Supplement 112-1, PacRim5 Special Issue, The Ceramic Society of Japan, 2004, pp. S248–S251.

[13] Y. Matsuura, K. Matsukawa, H. Inoue, Fabrication of polysilane–silica hybrid thin films with controlled refractive index, Chem. Lett. 30 (3) (2001) 244–245, http://dx.doi.org/10.1246/cl.2001.244, arXiv:https://doi.org/10.1246/cl.2001.244.

[14] R.S. Meltzer, S.P. Feofilov, B. Tissue, H. Yuan, Dependence of fluorescence lifetimes of Y 2 O 3: E u 3+ nanoparticles on the surrounding medium, Phys. Rev. B 60 (20) (1999) R14012.

[15] C. Tregidgo, J. Levitt, K. Suhling, Effect of refractive index on the fluorescence lifetime of green fluorescent protein, J. Biomed. Opt. 13 (2008) 031218, http://dx.doi.org/10.1117/1.2937212.

[16] R. Lampert, S. Meech, J. Metcalfe, D. Phillips, A. Schaap, The refractive index correction to the radiative rate constant in fluorescence lifetime measurements, Chem. Phys. Lett. 94 (2) (1983) 137–140, http://dx.doi.org/10.1016/0009-2614(83)87560-5, URL: https://www.sciencedirect.com/science/article/pii/0009261483875605.

[17] R. Mercadé-Prieto, L. Rodriguez-Rivera, X.D. Chen, Fluorescence lifetime of Rhodamine B in aqueous solutions of polysaccharides and proteins as a function of viscosity and temperature, Photochem. Photobiol. Sci. 16 (2017) 1727–1734.

[18] T. Zhang, Z. Zhang, X. Zhao, C. Cao, Y. Yu, X. Li, Y. Li, Y. Chen, Q. Ren, Molecular polarizability investigation of polar solvents: water, ethanol, and acetone at terahertz frequencies using terahertz time-domain spectroscopy, Appl. Opt. 59 (16) (2020) 4775–4779.

[19] M. Angelini, E. Manobianco, P. Pellacani, F. Floris, F. Marabelli, Plasmonic modes and fluorescence enhancement coupling mechanism: A case with a nanostructured grating, Nanomaterials 12 (23) (2022) http://dx.doi.org/10.3390/nano12234339, URL: https://www.mdpi.com/2079-4991/12/23/4339.

[20] F. Floris, C. Figus, L. Fornasari, M. Patrini, P. Pellacani, G. Marchesini, A. Valsesia, F. Artizzu, D. Marongiu, M. Saba, et al., Optical sensitivity gain in silica-coated plasmonic nanostructures, J. Phys. Chem. Lett. 5 (17) (2014) 2935–2940.

[21] S. Ma, S. Du, G. Pan, S. Dai, B. Xu, W. Tian, Organic molecular aggregates: From aggregation structure to emission property, Aggregate 2 (4) (2021) e96, http://dx.doi.org/10.1002/agt2.96, URL: https://onlinelibrary.wiley.com/doi/abs/10.1002/agt2.96. arXiv:https://onlinelibrary.wiley.com/doi/pdf/10.1002/agt2.96.

[22] J. Heo, D.P. Murale, H.Y. Yoon, V. Arun, S. Choi, E. Kim, J.-S. Lee, S. Kim, Recent trends in molecular aggregates: An exploration of biomedicine, Aggregate 3 (2) (2022) e159, http://dx.doi.org/10.1002/agt2.159, URL: https://onlinelibrary.wiley.com/doi/abs/10.1002/agt2.159. arXiv:https://onlinelibrary.wiley.com/doi/pdf/10.1002/agt2.159.

[23] Y.-Q. Wang, L. Li, J. Yin, X. Yu, X. Wu, L. Xu, Turn on fluorescence detection of curcumin in food matrices by the novel fluorescence sensitizer, Anal. Chim. Acta 1254 (2023) 341094.